Virtual Human Hand: Grasps and Fingertip Deformation

Esteban Peña-Pitarch(✉), Jesus Fernando Padilla Magaña, Neus Ticó-Falguera, Anas Al Omar, Iñaki Alcelay Larrión, and Jordi Vives Costa

Mechanical Engineering Department, Escola Politècnica Superior d'Enginyeria de Manresa (UPC), Av. Bases de Manresa, 61-73, 08242 Manresa, Spain
{esteban.pena, jesus.fernando.padilla, anas.al.omar, inaki.alcelay, jordi.vives}@upc.edu

Abstract. The objective of this paper is to simulate the human hand when grasping an object, considering the angles of the finger joints and the fingertip deformation. To study the grasp of an object used in activities of daily life (ADL) we focus on the equations given by grasps with force-closure. In this paper we address several topics and study grasping holistically, including power and precision grasping, the position of the finger and joint angles, fingertip deformation and fingertip forces (normal and frictional forces), and assess how all these features combine to perform a complete grasping action.

Conclusions: We describe the strategy used to solve the problem of calculating the force when grasping with five fingers; the same strategy is used in both power and precision grasps.

Keywords: Human hand · Grasping · Force closure · Fingertip force

1 Introduction

Power and precision grasps have already been studied in some detail in the literature.

While our paper shows the equations used to simulate how, in a virtual environment, a virtual hand grasps an object, [1] presented a method for evaluating the accuracy and precision of the joint angles as determined by a hand motion capture protocol using simultaneously collected static computed tomography (CT) images. Similarly, [2] proposed a new method for reconstructing the hand model for individuals, including link structure models, homologous skin surface models, and homogeneous tetrahedral mesh models in a reference posture. The effects of stimuli on deformations within the soft tissues of fingertips and the dependence of tactile sensation on the deformation while touching an object were investigated by [3], who developed a finite element method (FEM) based on the physiological structure of the fingertip to simulate the contact interaction between a fingertips and a flat plate.

A technique for stimulating finger-pad shear deformation transferred to the side of the fingertip was developed by [4]. For their part, [5] created a wearable sensor system for estimating finger contact force by measuring the mechanical deformation of the side of the finger-pad.

M. Di Nicolantonio et al. (Eds.): AHFE 2019, AISC 975, pp. 484–492, 2020.
https://doi.org/10.1007/978-3-030-20216-3_45

In order to simulate the skin contact deformation mechanism, a physical model based on the Boussinesq approximation with nonlinear elasticity and a compressing-swelling effect was proposed by [6].

[7] described a complete grasp model for simulating experiments in which a subject was asked to grasp two cylinders of different diameters and weights, with similar angles to those we use in our experiments we calculate with our research; similar results were also found by [8] using objects 3, 5, or 7 cm in diameter. Using an instrumented cylinder [9] described the magnitude of pinch force as the function of a cylinder allowing simultaneous measurements of the opposition axis of the index and the thumb of the hand. [10] introduced a paradigm in which subjects grasp the same final object from the same starting position, once as a typical laboratory task and once as a part of everyday behavior.

Using a tentative grasping posture and the most open posture during grasping as an input on an artificial neural network, [11] calculated hand posture prediction with a biomechanical model. [12] investigated where subjects place their digits on a bottle when the upcoming task (lift versus pour) and the object content (i.e. amount of liquid: empty, half-full, and full) were manipulated. To determine whether catch-up responses are elicited by unexpected rotational perturbation and are strength-, axis-, and/or direction-dependent [13] imposed step torque loads about each of two axes which were defined to the subject's hand in order to study the precision grip responses.

[14] presented a metric based on the evaluation of how many different postures or configurations a hand can perform by studying the reachable set of fingertip poses.

[15] developed a computer model able to predict the internal loading patterns of tendons and joint surfaces experienced by the human finger. They proposed a methodology based on a nonlinear optimizing mathematical technique with a criterion of boundary conditions and equality equations.

Through the analysis of a quasi-static model, [16] defined grasp structural properties related to contact force controllability and object manipulability.

[17] performed experimental measurements in 20 subjects to obtain a stiffness map of the different grasping contact areas of the human hand. A force-displacement apparatus was used to simultaneously measure force and displacement at 39 different points on the hand and six levels of force ranging from 1 N to 6 N.

[18] proposed a technique for calculating the coefficient of friction for fingertip-object interface. This technique is based on a 3D force sensor moved horizontally while subjects applied a specific normal force (4 N, 8 N, and 12 N) on the surface of a sensor covered with different materials (sandpaper, cotton, rayon, and silk).

The objective of the present study is to simulate the human hand when grasping an object, considering the finger joint angles and the fingertip deformation.

2 Design

Once the fingers make contact with an object and grasp it, they present appreciable deformation at the points of contact. The number of contacts depends on the type of grasp: power or precision. In general, each contact has three forces, one normal to the object's surface and two frictional forces, and another action, is the torsional moment.

Without losing generality, Fig. 1 shows a schematic view of the five fingertips (left) and four fingers (right), and the contact finger when precision grasping an object using five and four fingers.

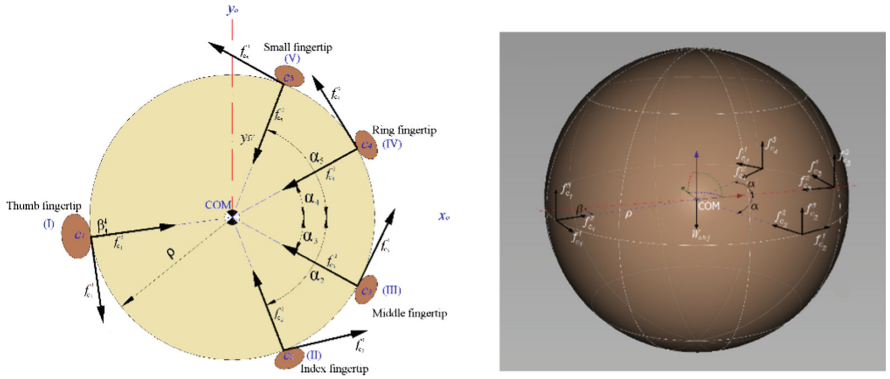

Fig. 1. Left, shows a schematic precision grasp with the five fingertip and the forces in the plane (x_0, y_0). Right, shows a ball grasped with precision in three dimensions with four fingers.

Figure 2 shows a power grasp of a cylinder, where I is one contact point of the thumb, II is for the index finger, III is for the middle finger, IV for the ring finger, and V for the small finger. Figure 2 shows points of contact and their locations with respect to

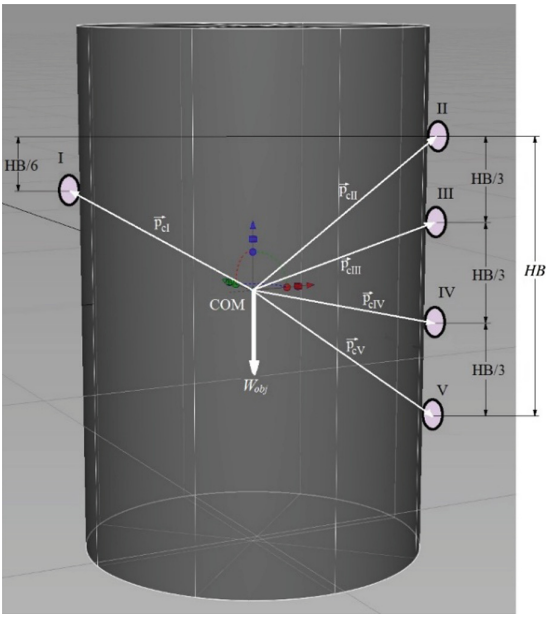

Fig. 2. Power grasp simulation using five fingers.

a center of mass (COM). Of course, the COM may vary depending on whether the object is full or empty, or depending on its mass distribution. $\vec{p}_{cI}$ is the skew-matrix for the thumb, $\vec{p}_{cII}$ for the index, $\vec{p}_{cIII}$ for the middle, $\vec{p}_{cIV}$ for the ring finger, and $\vec{p}_{cV}$ for the small finger. HB refers to the Hand Breath, shown in [20].

When a human hand grasps an object we consider as a static problem; we do not consider the manipulation of the object. On this assumption, we apply the grasping equations shown in [19].

Figure 3 represents an arbitrary finger, where ρ is the variable radius of the object grasped, ℓ_{m-2} is the length of the proximal phalanx, indicated by the number 2 and the fingers are represented by m: $m = I$ for the thumb, $m = II$ for the index finger, $m = III$ for the middle finger, $m = IV$ for the ring finger, and $m = V$ for the small finger.

$f_{c_i}^2$ is the normal force at contact c_i for the precision grasp, when the only contact point is the fingertip. In the power grasp, since we have more contact points in each finger than in the precision grasp, we use the sub-indices i, j, and k to indicate the contact points in the proximal, middle and distal phalanxes respectively.

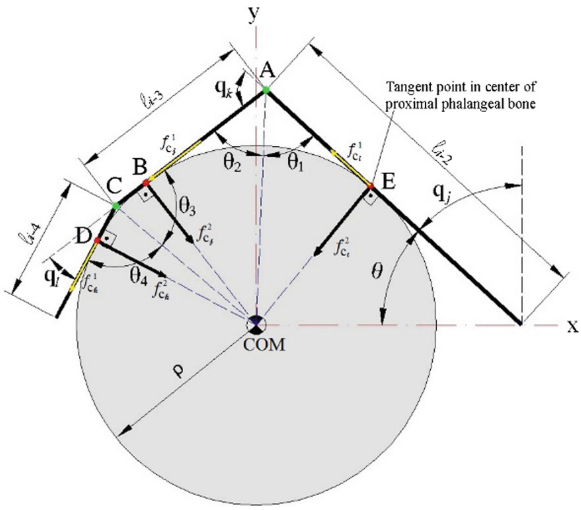

Fig. 3. Power grasp simulation. Cross section.

When grasping, the finger position is determined using a 25 degrees of freedom (DOF) hand model, from [20] and [21]. Once the object is grasped several positions are possible depending on the object's type and size, the task to be performed, its weight, and so on.

Figure 1 shows the relative position of the fingertip when grasping an object with the precision grasp. In this case, angles β, α_2, α_3, α_4, and α_5 vary according to the number of fingers used in the grasp, and the number of fingers used is a function of the radius ρ of the object being grasped.

Our approximation is based on the observation that when a precision grasp is used to grasp an object, the fingertip position forms a circle that is independent of the object's shape. For this reason, Fig. 1 shows the general position of the fingertip for any shape of the object.

In this observation based on ten healthy people all grasping an object with the thumb and the index, with angles $\beta = \alpha_2 = 0$, the other fingers do not participate. This is the case when the object diameter is $5 \leq \rho \leq 12.5$ mm. Similar observations are found when other fingers are used to grasp. Table 1 shows the values obtained depending on the number of fingers used and the cylinder with radius ρ.

In this case, our approximation is based on the fact that fingers have three contact points: the proximal phalanx, the middle phalanx, and the distal phalanx (Fig. 3). To calculate the geometric angles shown in Fig. 3, once the finger grasps the object we impose the position of point E in the middle of the proximal phalanx.

Once point E is known, the other angles can be determined from the geometrical position.

The angle θ in Fig. 3 is $\tan\theta = 2\rho/\ell_{i-2}$. If we impose the contact between the middle phalanx and the object is in $\left(\frac{2}{3}\right)\ell_{i-3}$, the angle θ_2 is $\tan\theta_2 = (3\rho)/(2\ell_{i-3})$, and $\theta_1 = \theta$.

Table 1. Angle range in function of the object radius (ρ) and the number of fingers used.

Radius object ρ (mm)	Number of fingers	Angle range	Symmetry
$5 \leq \rho < 12.5$	2	$\alpha_2 = \beta = 0$	
$12.5 \leq \rho < 20$	3	$0 \leq \beta \leq 8$ $0 \leq \alpha_2 < 30$	$\alpha_2 = \alpha_3$
$20 \leq \rho < 35$	4	$0 \leq \beta \leq 8$ $30 \leq \alpha_2 \leq 50$ $0 \leq \alpha_3 \leq 30$	$\alpha_4 = \alpha_3$
$35 \leq \rho < 70$	5	$0 \leq \beta \leq 8$ $40 \leq \alpha_2 \leq 80$ $0 \leq \alpha_3 \leq 30$	$\alpha_5 = \alpha_2$ $\alpha_4 = \alpha_3$

From this geometrical relationship the angles for each joint are:

$$\begin{aligned} \mathbf{q}_j &= 90 - \theta \\ \mathbf{q}_k &= 180 - \theta_2 - \theta_1 \\ \mathbf{q}_\ell &= \frac{2}{3}\mathbf{q}_k \end{aligned} \tag{1}$$

Where θ is obtained by the position of the ray proximal phalanx using the geometrical relationship, $\tan\theta = \rho/\ell_{i-2}$, and ℓ_{i-1}, ℓ_{i-2}, and ℓ_{i-3} are the lengths of the finger phalanx defined in [20].

To calculate the normal force exerted by each contact point we use finite element analysis. First, we use the nonlinear method since the fingertip has different layers with different Young's moduli.

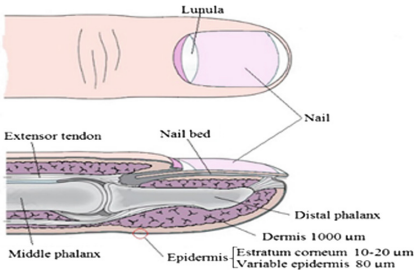

Fig. 4. Longitudinal cross-section displaying the dorsal and ventral proximal finger.

Figure 4 shows a longitudinal cross-section of the finger parts. The thickness of different layers shown in the figure is described in [22]. Here we reproduce part of Geeligs' schematic representation of the different skin layers, highlighting the ones that interest us most. These layers help us to define the three parts, in which each part has a Poisson's ratio and a Young's modulus.

3 Results

Figure 5 shows the variation of the joint angle for each finger when the cylinder radius decreased by three hand sizes based on hand length (HL). Using the nomenclature in [21], q_7, and q_8 are the angles for flexion/extension (F/E) for the metacarpophalangeal joint (MCP) and proximal interphalangeal joint (PIP) of the index finger; where q_9 represents the distal interphalangeal joint (DIP) which does not appear here, because $q_9 = \left(\frac{2}{3}\right)q_8$ is adopted from [24]. Similarly q_{11} and q_{12} are for the middle finger and for the same joints MCP and PIP, q_{17} and q_{18} for the ring finger, and q_{23} and q_{24} for the small finger. The thumb is not mentioned because in the experiments it remained in the neutral position. No joint presented any abduction/adduction (Ab/Ad).

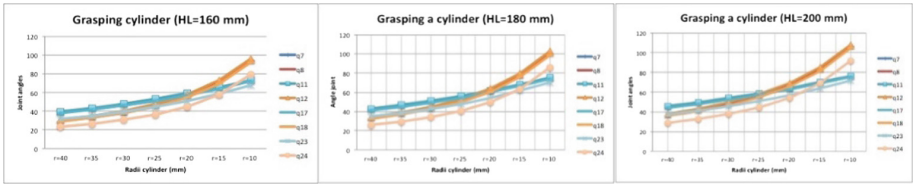

Fig. 5. Relationship between cylinder radius and joint angle for each finger when the cylinder radius decreased. Three hand sizes based on hand length (HL).

Experiments to measure the maximum deformation of the fingertip found the maximum displacement obtained on the z axis (vertical) to be 3.25 mm. These results are similar to the ones obtained by [23].

The strain obtained in both cases using the finite element method and the experiment carried out with an actual finger, when applying vertical forces directed towards the finger of 1 N and 6 N [25].

4 Discussion

In this paper we address several topics and study grasping holistically, including power and precision grasping, the position of the finger and joint angles, fingertip deformation and fingertip forces (normal and frictional forces), and assess how all these features combine to perform a complete grasping action.

We use results from [26], in which the authors examined the effect of the friction between the hand and grip surface on a person's grip strategy and force generation capacity.

Once the object is grasped, the point at issue is whether its weight and shape are adjusted to the user. To answer this question, we study the angles of each joint of the hand, based on a 25 DOF virtual model hand. The deformation of the fingertip allows us to calculate the normal forces exerted by each point of contact. We show that the points of contact of the hand depend on the object size, hand size, and the type of grasp (power or precision).

Based on our observations, we suppose that when an object is grasped with precision, regardless of the fingers used, forms a circle containing two, three, four, or five opposite points. With this idea in mind we know that the angles described in Fig. 1.

Figure 5, left, shows the joint angles for each finger. The horizontal axis shows the radius of the cylinder grasped. With a radius $\rho = 40$ mm the joint angles are between 20 to 40°; this means that for this radius the angle varies only a small angle amount around the neutral position, that is 30°, as shown in [20]. On the other hand, when the cylinder radius is $\rho = 10$ mm the joint angles range between 65 to 95°; therefore, the joint angles are larger if the object is small and smaller if it is large. Figure 5, middle and right shows a similar tendency. The difference depends on the size of the hand; a user with a $HL = 200$ mm must close the hand around the object with a slightly larger joint angle, between 35 to 50°, with the $HL = 180$ mm the joint angles vary between 25 to 42°.

The deformation begins with a neutral position of 15 mm measured on the z-axis and a maximum displacement in the same axis of 3.25 mm. The forces are between 1 N to 6 N and the Young's modulus varies between 34 kPa to 200 kPa [25].

5 Conclusions

In this paper we present a virtual human hand in a full grasping action. We describe the strategy used to solve the problem of calculating the force when grasping with five fingers; the same strategy is used in both power and precision grasps. Once we

calculate the normal force for each finger, we can calculate all the friction forces and torsional friction forces for a soft fingertip if we know the weight of the object W_{obj}. Additionally, we to need know the joint angles and we calculate them with the forward and inverse kinematics in the references described above.

We see too how the angles of each joint vary with hand length and the size of the object (radius ρ). The Poisson's ratio did not vary significantly and we adopted an average of Young's modulus of 65 kPa.

In future studies we will apply these equations and solution in a subject with a pathology, such as stroke, and simulate their evolution after six months. This focus will allow us to implement a model of the evolution of the able to predict the evolution unhealthy/injured hand, giving the ergonomist new tools to design equipment for facilitating activities of daily life.

Subsequent versions of our model of the virtual human hand will incorporate the muscles and their effect on the hand's action.

Practical implications:

- New tools to design equipment for facilitating activities of daily life.
- Application in several sports to design and study the impact grasp force to the users.
- Tools to design a predictive model of evolution unhealthy/injured hand

Acknowledgments. This work was partially supported by the Spanish government (DPI2016-80077-R).

References

1. Buffi, J., Sancho-Bru, J.L.: J. Biomech. Eng. **136**, 1–6 (2015)
2. Endo, Y., Tada, M., Mochimaru, M.: J. Comput. Design Eng. **1**, 1–12 (2014)
3. Hu, J., Xin, D., Wang, R.: World J. Model. Simul. **3**, 73–78 (2007)
4. Matsuura, Y., Okamoto, S., Yamada, Y.: Lecture Notes in Computer Science, vol. 8619, pp. 313—319 (2014). ISSN 16113349
5. Nakatani, M., Kawasoe, T., Shiojima, K., Koketsu, K., Kinoshita, S., Wada, J.: IEEE World Haptics Conference, pp. 323–328 (2011)
6. Xie, Y., Kanai, S., Date, H.: Key Eng. Mater. **530**, 675–680 (2013)
7. Sancho-Bru, J.L., Mora, M.C., León, B.E., Pérez-González, A., Iserte, J.L., Morales, A.: Computer methods in biomechanics and biomedical engineering 37–41 (2012)
8. Bongers, R.M., Zaal, F.T., Jeannerod, M.: Hum. Mov. Sci. **31**, 487–501 (2012)
9. Bourbonnais, D., Frak, V., Pilon, J.F., Goyette, M.: J. Neuroeng. Rehabil. **5**, 2 (2008)
10. Bock, O., Züll, A.: Hum. Mov. Sci. **32**, 249–256 (2013)
11. Mora, M.C., Sancho-Bru, J.L., Perez-Gonzalez, A.: Int. J. Adv. Robotic Syst. **1** (2012)
12. Crajé, C., Lukos, J.R., Ansuini, C., Gordon, A.M., Santello, M.: Experimental brain research. Experimentelle Hirnforschung. Expérimentation cérébrale. **212**, 119–124 (2011)
13. De Gregorio, M., Santos, V.J.: J. Biomech. **46**, 1098–1103 (2013)
14. Feix, T., Romero, J., Ek, C.H., Schmiedmayer, H.B., Kragic, D.: IEEE Trans. Robot. **29**, 82–93 (2013)
15. Fok, K.S., Chou, S.M.: J. Biomech. **43**, 701–713 (2010)

16. Prattichizzo, D., Malvezzi, M., Gabiccini, M., Bicchi, A.: IEEE Trans. Robot. **29**, 1440–1456 (2013)
17. Pérez-González, A., Vergara, M., Sancho-Bru, J.L.: J. Biomech. **46**, 2644–2650 (2013)
18. Savescu, A.V., Latash, M.L., Zatsiorsky, V.M.: J. Appl. Biomech. **24**, 43–50 (2010)
19. Murray, R.M., Li, Z., Sastry, S.: A Mathematical Introduction to Robotic Manipulation, 1st ed. Robotics (1994)
20. Peña-Pitarch, E.: Virtual Human Hand: Grasping Strategy and Simulation. Ph.D. thesis Universitat Politecnica de Catalunya (2008)
21. Peña-Pitarch, E., Ticó-Falguera, N., Yang, J.: Comput. Methods Biomech. Biomed. Eng. **17**, 568–579 (2014)
22. Geerligs, M.: Skin layer mechanics. Ph.D. thesis Universiteitsdrukkerij TU Eindhoven, Eindhoven, The Netherlands (2009)
23. Shimawaki, S., Sakai, N.: J. Environ. Eng. **2**, 56–63 (2007)
24. Rijpkema, H., Girard, M.: Comput. Graph. **25**, 339–348 (1991)
25. Peña-Pitarch, E., Ticó, N., Lopez, J.A., Al Omar, A., Alcelay, J.I.: Driving device for a hand movement without external force. Mech. Mach. Theory **105**, 388–396 (2016)
26. Enders, L.R., Seo, N.J.: J. Biomech. **44**, 1447–1453 (2011)